

A numerical study of quasi-geostrophic flow over isolated topography

By J. VERRON AND C. LE PROVOST

Institut de Mécanique de Grenoble, Grenoble

(Received 12 July 1983 and in revised form 14 November 1984)

An extensive set of numerical simulations is performed to synthesize the behaviour of a barotropic flow over isolated topography on an f -plane and on a β -plane. The model is based on the quasi-geostrophic vorticity equation, where the dissipation terms have been retained. The use of open boundary conditions, following the method described by Orlanski (1976), allows detailed simulation of time-dependent flows over long periods.

On the f -plane, the ultimate solution is always characterized by a typical vorticity field with an anticyclonic vortex trapped over the topography, but different transient regimes occur, related to the importance of advection versus topography effect: direct advection of the positive vortex for strong flows; eddy interactions and double-vortex-structure appearance for weaker flows; oscillatory regimes with topographic trapped-waves generation for very strong vorticity-interaction cases.

On the β -plane, and for prograde flows, the situation is complicated by a Rossby wave pattern extending mainly downstream but also having an upstream component corresponding to zonal waves. For retrograde flows the obstacle does not excite Rossby waves but a transient response with zonal waves whose lifetime depends on the nonlinearity.

1. Introduction

Since the pioneering work of Proudman (1916) and Taylor (1917), many studies have been made on the typical property of a flow in a rapidly rotating system independent of the coordinate parallel to the axis of rotation. Although the existence of the so-called Taylor columns supposes that the flow is steady, inviscid and homogeneous, it seems pertinent to conjecture a physical relevance of this type of phenomenon to geophysical situations, especially in the ocean. Such approaches are strongly relevant to the increasing interest in studying topographic effects: in the ocean, bottom topography is thus suspected to be a possible eddy source for meso-scale and large-scale flows, and possibly to influence the mechanisms of barotropic and baroclinic instabilities. In many areas, oceanographic data suggests that submarine topography plays this important role. Concerning the mesoscale, we can refer to the observations of Meincke (1971), Vastano & Warren (1976), Owens & Hogg (1980), Richardson (1980), Gould, Hendry & Huppert (1981) etc. which can be related to the Taylor-column problem.

Following Hide (1961), who conjectured that Jupiter's Great Red Spot was a manifestation of a Taylor column, many investigations have been undertaken, both theoretical and experimental, to understand and extend this concept in a more realistic context. Hide & Ibbetson (1966) and Hide, Ibbetson & Lighthill (1968)

published experimental studies extending the original Taylor experiments. It was established in particular that, in laboratory situations, the fluid within the column was never stagnant but had a more complex structure. More recently, new experiments by Vaziri & Boyer (1971), Davies (1972), Boyer & Davies (1982) and Boyer, Davies & Holland (1984) refined the knowledge of controlling parameters and viscous effects in the Taylor column. Some of these recent studies, and others from Vaziri (1977), and McCartney (1975) include the β -effect. A good survey of laboratory experiments in the field was published by Baines & Davies (1980) both for homogeneous and stratified flows.

Ingersoll (1969) presented the first nonlinear analytical calculations, based on the conservation of potential vorticity in steady quasi-geostrophic flow. This work was extended by Huppert (1975) who gives a criterion for Taylor-column formation with axisymmetric obstacles in the f -plane quasi-geostrophic hypothesis. The flow is shown to be deviated by the topography, on the left and then on the right, looking downstream, and with a fore-and-aft symmetry. The vorticity field is characterized by an anticyclonic eddy trapped on the topography. Johnson (1978*a*) points out the existence of a steady solution to the finite-Rossby-number equations of motion corresponding to a situation where two vortices of opposite signs are trapped by a right circular cylinder in a uniform stream. The negative vorticity is located over the topography and the patch of positive vorticity is shifted rightward (looking downstream). Kozlov (1981) generalized the calculation of the cyclonic eddy position for other topographies.

The first to examine the effect of variable Coriolis parameter was Ingersoll (1969), for a westward flow and large β . McCartney (1975) obtained analytical solutions of the inertial quasi-geostrophic β -plane equations for a steady two-layer flow with moderate stratification; in this work, the homogeneous single-layer case is also considered, as a limiting case. For eastward flows, he found a meandering stationary wake downstream of the bump, and determined the influence of β on Taylor-column occurrence and position. Hogg (1973), McCartney (1975) and Johnson (1977, 1979) included stratification in their approaches; it could be shown that the continuously stratified Taylor column looks like a conical vortex of height sufficient to reach the free surface.

The non-stationary aspect of this class of problems was first investigated by Huppert & Bryan (1976); with a numerical model they looked at the flow initiation of a stratified fluid over an isolated seamount on the f -plane, neglecting bottom friction. Their model is three-dimensional with nine levels in the vertical and has periodic horizontal boundaries. The flow is started from rest and, during the time of their simulation, they found two regimes, depending on the amplitude of the incoming flow velocity. They interpreted their results by using rather simple analytical calculations based on an approximate representation of their stream functions in terms of line vortices. With this model they predicted, for a given topography, the transition between the two kinds of regimes. However, because of the periodic boundary conditions used, these numerical simulations had to be stopped when the perturbations drifting downstream reappeared upstream, making it difficult to obtain long-term solutions.

More recently, James (1980) included downstream boundary conditions which allowed vorticity to be advected smoothly out of the domain: this study was devoted in particular to the topography-induced forces in both steady and transient situations.

The aim of this paper is to synthesize the different typical responses of a

quasi-geostrophic homogeneous flow impinging on an isolated seamount by using an open-boundary numerical model, and to point out the transient or steady characteristics of the observed features. The use of upstream and downstream radiative boundary conditions makes it possible to follow the evolution of the transient response of the flow over long periods of time on the f -plane, and the β -plane. The homogeneous quasi-geostrophic restriction of the problem allows a large set of characteristic parameters in oceanic flows to be covered without excessive computing cost. Section 2 gives the details of the model and the boundary conditions used, and §3 analyses the typical parameters of the problem. Section 4 describes the different numerical solutions obtained in the f -plane approximation in relation to the advection and vorticity interaction effects; the initiation processes and the steady solutions are examined and discussed. Section 5 is related to the contribution of the planetary vorticity gradient in the present framework: the existence of Rossby waves is pointed out in addition to the previous typical responses of flows.

2. The model

2.1. Description

We consider the flow of a barotropic fluid in a rectangular oceanic box. The domain has two solid boundaries and two open boundaries; generally the first ones are situated north and south and the second ones east and west, so that the domain looks like a zonal channel. Horizontal dimensions are denoted by LX and LY and the depth of fluid is scaled by D (figure 1). The bottom topography is measured by its deviation $h(x, y)$ above the sea floor ($z = -D$). The whole system is rapidly rotating: the Coriolis parameter f varies with latitude y so that its value is f_0 for the mid-latitude.

Initially the fluid is at rest and at time $t = 0$ a pressure gradient in the y -direction is introduced in such a way that a mean flow is generated in the x -direction. Alternatively, we start from a uniform flow and at $t = 0$ the topography rises, instantaneously or progressively during the first timesteps. These two initial conditions are equivalent provided that the initiation timescale is much smaller than the flow timescale.

2.2. Governing equations

The two fundamental assumptions used here are the homogeneous fluid and the quasi-geostrophic hypothesis. The barotropic behaviour of the flow is a strong constraint in comparison to the real ocean. An overestimation of the topographic effect will be present, due to the hypothesis that horizontal velocity is not depth dependent.

The Rossby number ϵ is defined as:

$$\epsilon = \frac{U}{f_0 L},$$

where U and L are velocity and length characteristic scales of movement. In the scale of our model, ϵ is small and justifies the quasi-geostrophic approximation used. Moreover, we require that the relative depth D/L and the ratio L/a (where a is the Earth radius) are also small and of order ϵ (Pedlosky 1979). This leads to the linearization of the Coriolis parameter and then to the β -plane approximation. The quasi-geostrophic analysis of mesoscale oceanic flows shows the consistency of the rigid-lid assumption, as we look at planetary movements with large period compared to the Earth's rotation; gravity waves and Kelvin waves are thus filtered.

The purely geostrophic balance near a steep topography implies that motion is

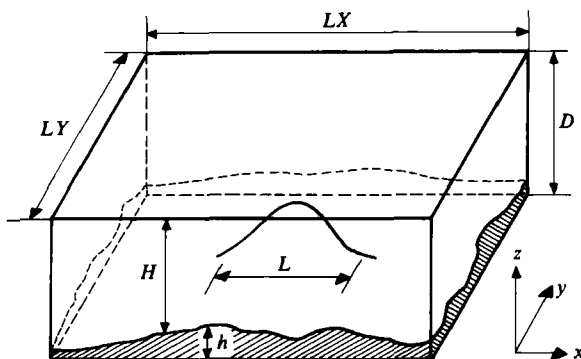


FIGURE 1. System geometry.

along the isobaths. In this paper we are interested in cases where this constraint is not present; thus we suppose the relative topography height is not too big compared to the local Rossby number.

Under these conditions, the equations of the problem are:

$$\frac{\partial \xi}{\partial t} + J\left(\psi, \xi + \beta y + \frac{h}{\epsilon D}\right) = -r\xi + D_t, \quad (1)$$

$$\xi = \Delta\psi, \quad (2)$$

ξ is the vorticity and ψ the stream function ($u = -\partial\psi/\partial y$, $v = \partial\psi/\partial x$). All the variables are non-dimensionalized; the timescale is chosen as the advection timescale L/U .

In the present model we use two different parametrizations for the last term D_t which represents lateral friction:

– the ‘Laplacian’ lateral friction

$$D_t = A \nabla^4 \psi, \quad A > 0,$$

with $A = 1/Re = A_H/UL$, where A_H is the classical horizontal turbulent viscosity and Re a horizontal Reynolds number;

– the ‘biharmonic’ lateral friction

$$D_t = A_4 \nabla^6 \psi, \quad A_4 < 0,$$

which acts as a kind of filter for the enstrophy contained in the small scales. The parameter r characterizes the bottom friction.

2.3. Numerical scheme

The numerical scheme is based on a classical finite-difference method. Second-order difference approximations are used for both space and time derivatives. The vorticity equation (1) is discretized using a leapfrog scheme which assures a second-order accuracy. The nonlinear term $J(\psi, \xi)$ is represented by simple central differences in time and with the Arakawa’s (1966) form in space which conserves vorticity, energy and enstrophy when integrated on a closed domain. The dissipative terms will induce numerical instability. For this reason the bottom friction is evaluated through a semi-implicit scheme, averaging the values at the preceding and succeeding time levels; likewise the D_t term is always lagged one time-step. The Laplacian terms are calculated by following the classical five-points procedure. The stream function ψ

and the relative vorticity ξ are computed at the same gridpoints separated by distances Δx and Δy . Except for special tests the mesh spaces are the same in both directions and have 5 or 10 km dimensional lengths. The finite-difference version of the Poisson equation (2) is solved using an NCAR subroutine package employing an FFT method with cyclic reduction (Hockney 1971). The successive evaluation of ξ at each time-step is simply deduced from (1).

2.4. Boundary conditions

Each calculation of ψ and ξ for the interior points requires a knowledge of boundary data everywhere. The boundary vorticity needs to be calculated after the interior vorticity and the stream function. On the other hand, the boundary stream function needs to be known before any calculation at each time-step.

The chosen boundary conditions on solid boundaries such as north and south walls are:

- to keep constant values of the stream function ψ in such a manner as to impose a constant flow rate through the domain: we impose a constant stream function on the north wall $\psi = \psi_N$ and on the south wall $\psi = \psi_S$;
- to use a slip condition for the boundary vorticity ($\xi = 0$).

For the open boundaries, the problem is more difficult because we want the upstream and downstream computational boundaries to be transparent to signals impinging on them. The use of open boundary conditions is of great interest for the numerical simulations of local dynamics. That is particularly the case in the field of oceanography where local processes have to be understood on their own, but with dynamical connections to the surrounding area. The ideal condition needed on the boundaries would allow perturbations generated inside the domain to go through the boundary without being distorted and without modifying the interior solution and its further evolution in time. As Orlanski (1976) states, the appropriate formulation depends largely upon the characteristic equations to be simulated. A variety of methods have been developed to achieve open boundary conditions in many cases, and especially when the problem is characterized by a hyperbolic equation, which is a typical feature of many ocean mesoscale problems. The most widely used are derived from the Sommerfeld radiation condition for the waves:

$$\frac{\partial \phi}{\partial t} + c \frac{\partial \phi}{\partial x} = 0. \quad (3)$$

Kreiss (1966) was among the first to implement this condition in considering the perturbation to be radiating outside the domain like a single wave with phase velocity $c = \Delta x / \Delta t$. When the numerical solution is wavelike with a phase velocity close to the numerical velocity $\Delta x / \Delta t$ this method works quite well. But, the equations of mesoscale processes are nonlinear, the perturbations are not waves and, even if they were, the dispersion characteristics are not known. Orlanski improved the approach by calculating a local and instantaneous propagation velocity close to the boundary from the neighbouring interior gridpoints using a leapfrog finite-difference representation of the radiation condition. This propagation velocity is computed at each time-step and is different from point to point at the open boundary. For each boundary gridpoint the variable is estimated through radiation conditions by using this local velocity. The calculation can be done for each variable involved in the problem. With that successive-approximation numerical process, the real disturbance can thus be propagated. As Orlanski notes, the boundary conditions do not depend upon global quantities such as mean-flow properties.

In the present work, we use that procedure. Because topography primarily acts as a vorticity disturbance and the vorticity equation is hyperbolic, we compute a propagation velocity of the perturbation at each gridpoint next to the boundaries from the vorticity ξ :

$$V = \frac{\xi_{B-1}^{K-2} - \xi_{B-1}^K}{\xi_{B-1}^K + \xi_{B-1}^{K-2} - 2\xi_{B-2}^{K-1}},$$

where K is the time index, and B , $B-1$, and $B-2$ represent a boundary grid-point and its first and second normal interior neighbours. This velocity is then used to obtain ξ at the corresponding open-boundary gridpoints, upstream and downstream. The stream function is evaluated with the same propagation velocity computed from the vorticity field. Calling ϕ the variable to be estimated the boundary value then will be:

$$\phi_B^{K+1} = \frac{1-V}{1+V} \phi_B^{K-1} + \frac{2V}{1+V} \phi_{B-1}^K.$$

On condition that the mesh is sufficiently refined, this method appears to work successfully, as can be seen from figures 2, 12 and 13.

3. Parameters

Some of the parameters are the same for all the numerical experiments: the rotation parameters $f_0 = 10^{-4} \text{ s}^{-1}$, $\beta_0 = 2 \times 10^{-11} \text{ m}^{-1} \text{ s}^{-1}$ and the fluid depth $D = 4000 \text{ m}$. The other parameters vary from experiment to experiment. However, looking at (1) and (2), it is clear that only a few non-dimensional parameters have to be considered. Each of these non-dimensional parameters represents a dynamical effect:

- $\mu = \frac{h_m}{\epsilon D}$, the topography dynamical effect, based on the maximal topography height h_m ;
- β , the planetary vorticity gradient;
- r , the bottom friction;
- A , the lateral friction.

Every physical mechanism is concentrated through these four parameters.

The parameter μ implies that the topography height does not play an independent role but has to be related to the dynamical effect characterized by the Rossby number ϵ . The quasi-geostrophic frame in which we are supposes, in addition to the smallness of ϵ , that the relative height h/D is of order ϵ so that $\mu = O(1)$. The topography slope has also to stay smooth enough so that $|\nabla h| = O(D/L)$. The bump shape is chosen as circularly symmetric Gaussian:

$$h(x, y) = h_m e^{-(r/R)^2}$$

with $r^2 = (x-x_0)^2 + (y-y_0)^2$ and $R = \frac{1}{2}L$. The range of h_m is between 20 m and 800 m and we consider two different topography 'diameters': 40 km and 100 km. According to this diameter, the domain width LY is either 250 km or 500 km, and the domain length $LX = LY$ or $2LY$. The value of the mean flow velocity U is varied between 0.01 m s^{-1} and 0.1 m s^{-1} (in both eastward and westward directions). It follows that the topography parameter μ will be varied up to about 30.

The parameter $\beta = \beta_0 L^2/U$ is a measure of the dynamical importance of β , which represents all the spherical effects acting on the flow. In a barotropic model it operates like a topographic effect, i.e. a slope pitching down equatorward. A physically relevant value for the bottom-friction coefficient r is difficult to determine in the

oceanic context, but we expect $r < O(1)$. For the lateral friction, we chose a viscous timescale of the order of that at the spacescale of the grid.

In the ocean the most energetic timescales are in the range of a few days to a few months (Schmitz & Holland 1982). In comparison, that advective timescale associated with a seamount of scale L is L/U , that is to say of the order of ten days for mesoscale topography. Consequently, it appears that the study of transient flows at these timescales can be as relevant as the study of steady flows.

4. f -Plane flow

In the following section we suppose $\beta = 0$: the effect of the planetary vorticity gradient is not taken into account. This case corresponds to most of the previous studies on the subject described in the introduction. It is relevant to real problems if the topography has restricted horizontal scale.

Three successive stages can be distinguished:

- the initiation period ($t < L/U$) which is roughly common for all flows;
- the intermediate period ($t = O(L/U)$) which can last a few times the timescale L/U and where the flow looks well diversified in terms of input parameters and time;
- the final stage where the flow becomes steady ($t \gg L/U$).

The initiation of a flow above an isolated seamount was first described by Huppert & Bryan (1976). Although they considered stratified fluid, they did not seem to observe behaviour specifically associated with stratification (for the duration of the tests they investigate): with a homogeneous fluid the mechanisms are basically the same. In the first time-steps two eddies are created on the topography, the upstream eddy is associated with negative vorticity, the downstream eddy with positive vorticity. This first period can easily be interpreted in terms of vortex stretching or compression.

This situation changes rapidly and the two eddies rotate clockwise around the hill. Then a combination of several mechanisms occurs which determines the further flow evolution with time. They are dominated by two principal mechanisms:

- vorticity interaction which corresponds to nonlinear processes and is a function of topographic and incoming flow characteristics;
- advection processes whose intensity is a function of the strength of the incoming flow.

Different regimes are possible, depending on the relative importance of these two effects, but also on dissipation, occurrence of closed streamlines, etc. In the following, we present the main typical solutions, and we analyse energy and enstrophy variations to obtain a synthetic view.

4.1. Typical solutions

Strong advection (μ small)

When the velocity of the incoming flow is strong enough and the topography not too high, the advection process plays the dominant role. The cyclonic eddy is influenced by the mean flow which tends to advect it downstream, while the anticyclonic eddy remains in the vicinity of the seamount, slowly moving closer to the topographic axis. An example is presented in figure 2, with vorticity patterns. We notice that the open-boundary model works well for this kind of transient flow, since the cyclonic eddy can pass through the boundary without undergoing distortion and without influencing the subsequent development of the interior flow.

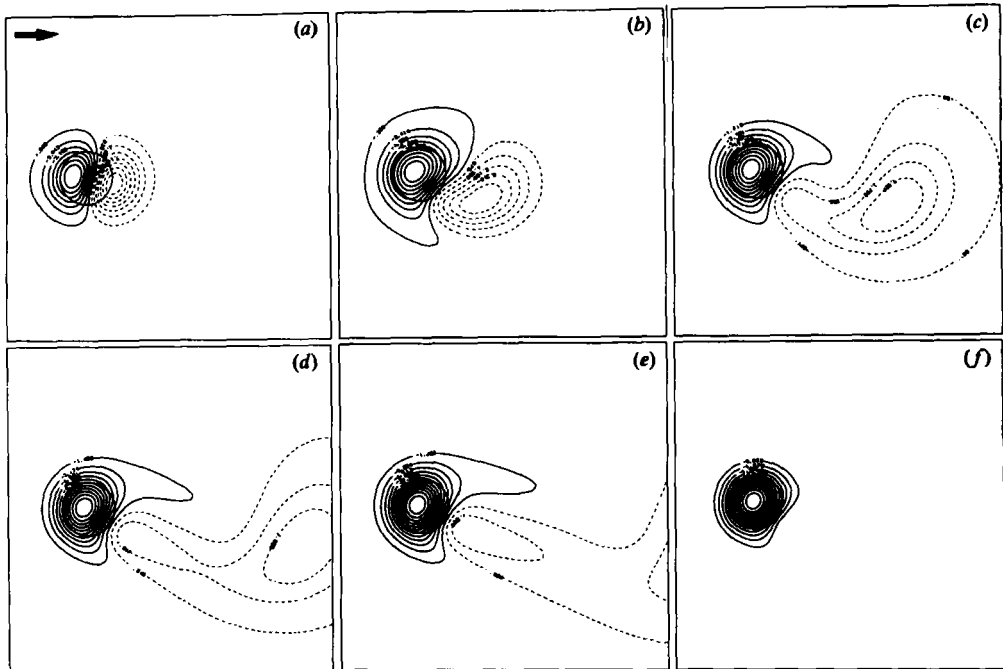


FIGURE 2. Vorticity field, strong advection effect: $\mu = 4$; $\beta = 0$; $r = 0$; $A = 0.025$.
 (a), at time $T = 0.36$; (b), 1.44; (c), 2.88; (d), 4.32; (e) 5.76; (f), 7.20.

After some advection time, all that remains in the domain is the anticyclonic eddy trapped on the topography. We reached a solution very close to the analytical solution of Huppert (1975) with an induced vorticity which is defined by:

$$\xi = -\frac{h}{\epsilon D},$$

when no closed streamline exists. We can easily deduce that, in this case, the dimensional induced vorticity is independent of the velocity U :

$$\xi^* = -\frac{f_0 h}{D}.$$

Thus topography will produce a vorticity disturbance whose intensity is independent of the mean flow.

Such configurations are obtained when the topography parameter is such that:

$$0 < \mu < \mu_d.$$

From our tests, $\mu_d \approx 11$. It must be noticed that this range of values includes the value μ_c characteristic of Taylor-column appearance (with a Gaussian topographic profile, the critical corresponding μ_c is found to be $\mu_c \approx 6.3$). Figure 3 shows the type of solution when $\mu_c < \mu < \mu_d$ and we can see the trapping of closed streamlines on the bump.

Strong vorticity interaction (μ large)

When the induced vorticity is strong enough compared to the advection effect, i.e. for growing values of μ , the cyclonic eddy remains first in the vicinity of the topography: after a rotating movement the two eddies stay trapped in the transverse

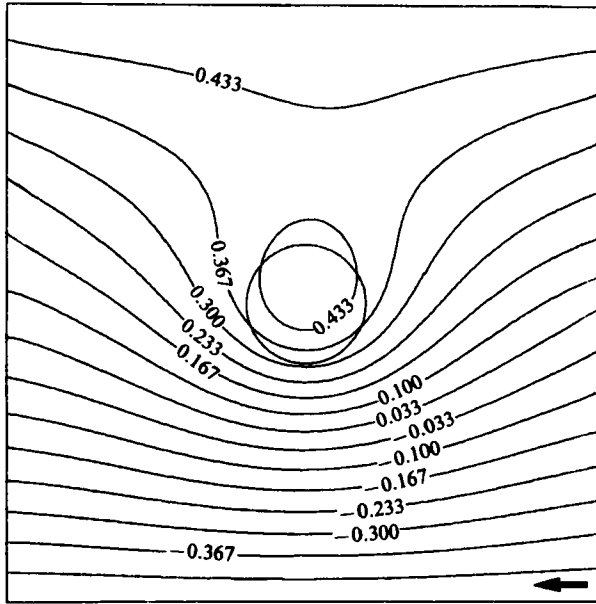


FIGURE 3. Streamlines, quasi-steady state with Taylor column: $\mu = 10$; $\beta = 0$; $r = 0$; $A = 0.001$; $T = 5.76$.

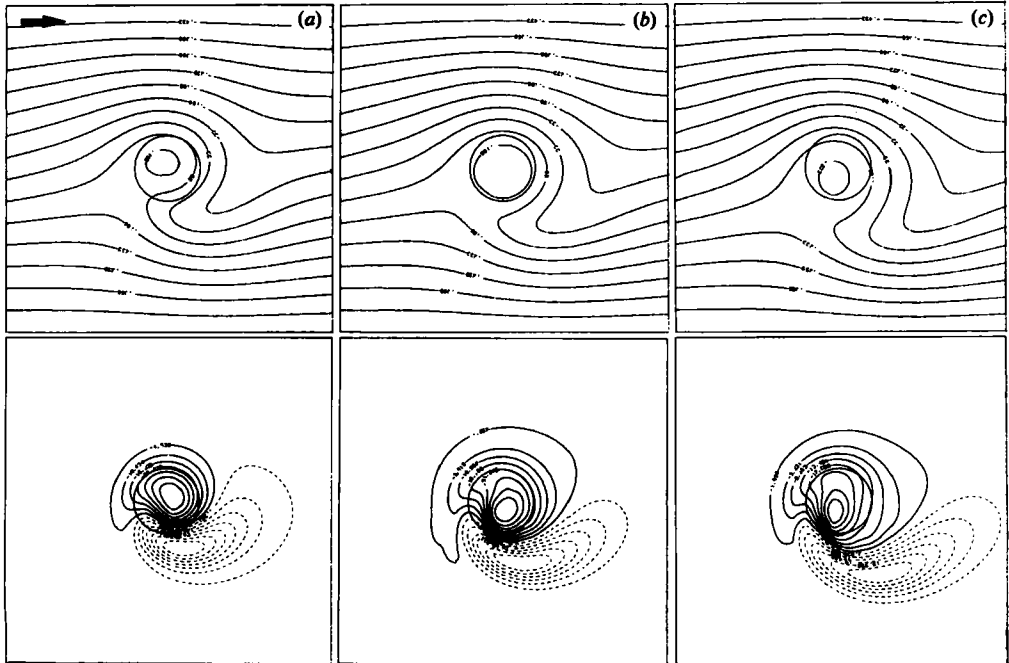


FIGURE 4. Streamlines and vorticity field, trapped paired eddies: $\mu = 12.5$; $\beta = 0$; $r = 0$; $A = 0.01$. (a), at time $T = 0.92$; (b), 1.38; (c), 1.84.

direction (figure 4). In all cases the cyclonic eddy centre is shifted from the bump on the right side of it, looking downstream. Such a flow can be stable during a time of order L/U . Beyond this time the positive vorticity structure is progressively advected by the main flow and leaves the domain through the open boundary, as in all the previous cases, when bottom friction is absent or weak. This holds in all

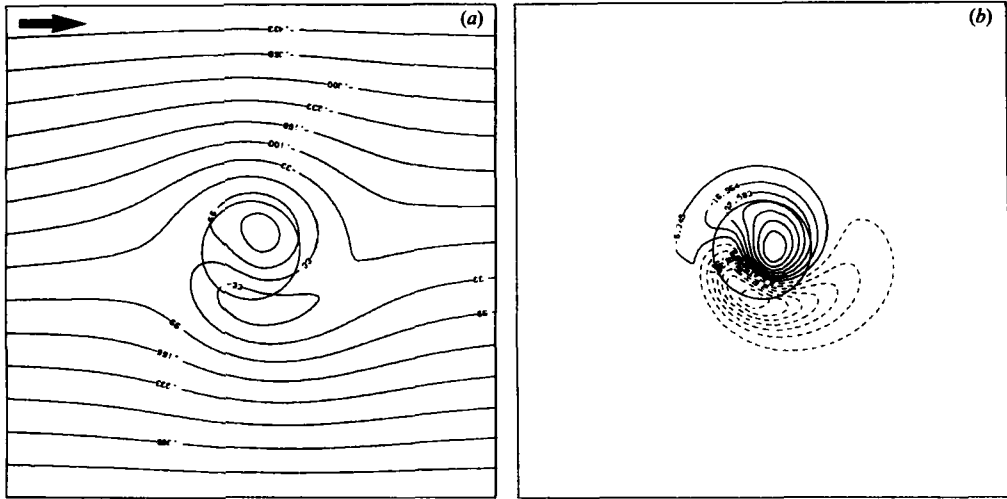


FIGURE 5. Streamlines and vorticity field, trapped paired eddies:
 $\mu = 15.6$; $\beta = 0$; $r = 0$; $A = 0.02$; $T = 1.15$.

the cases studied whatever μ may be. The only way to get a steady solution with the two eddies trapped on the topography would be if there were strong (unrealistic) bottom friction.

If the correct flow parameters are taken we can obtain transient solutions similar to Johnson (1977, 1978) and Kozlov (1981) steady solutions: the flow looks like a potential flow generated by a vortex pair. Figure 5 shows such an example in a typical case where two closed streamline zones are present corresponding to two Taylor columns.

The previous cases are obtained for μ greater than the critical value μ_d . If we continue to increase this parameter, the vorticity interaction is enhanced and we observe also a larger but unstable closed streamline pattern, which gives a more complex type of configuration. In a first stage the flow presents a strong analogy with the preceding cases. The two eddies interact and come to a transverse position, but the cyclonic eddy goes quickly beyond the median position and is enwrapped in the anticyclonic eddy. This situation is unsteady and it appears to be an oscillatory regime where the eddies' centres are oscillating on both sides of the topography. After a time, stabilization occurs when the cyclonic eddy is escaping downstream and advected outside the topography area and then the domain. Often the oscillation of the two vorticity cells is not complete and a strong eddy interpenetration and a splitting of vorticity structures in smaller scales can be observed: then a part of the cyclonic structure can go round the hill while the remaining part oscillates. The process goes on with a coalescence of the different patches of vorticity and begins again. The sketches in figure 6 show the successive mechanism. James (1980) has already mentioned this extreme behaviour with a similar model including bottom friction. Here, the experiments are carried out with and without bottom damping.

4.2. Energy and enstrophy disturbances

The topographic flow disturbance is measurable through integrated quantities like the energy and the enstrophy all over the domain. In non-dimensional form, we define

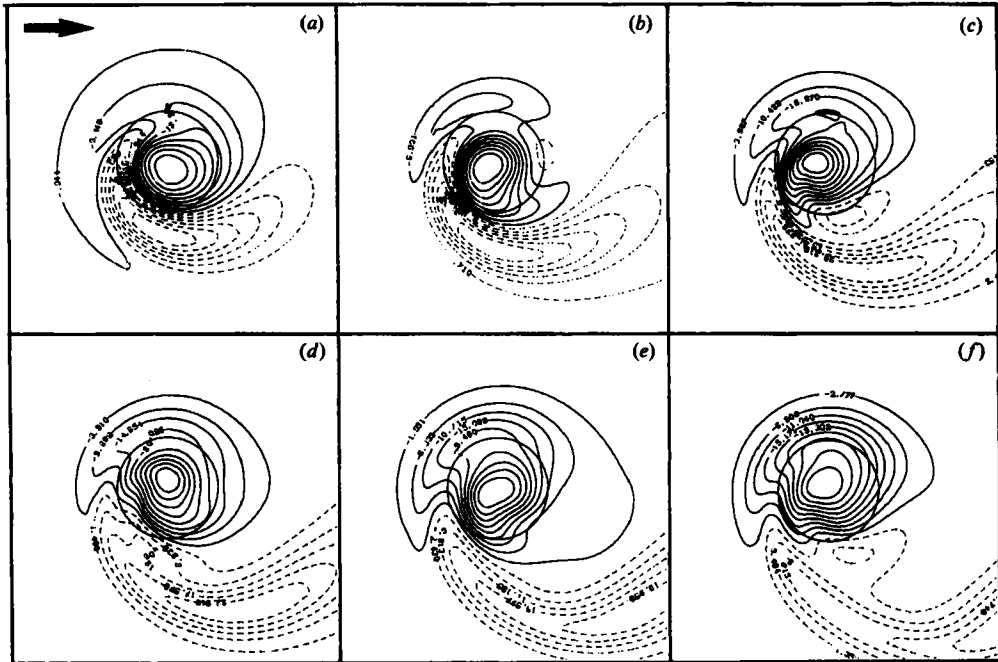


FIGURE 6. Vorticity field, circular trapped waves; $\mu = 18$; $\beta = 0$; $r = 0$; $A = 0.005$; at time $T = 1.080$ for (a), and timestep $\Delta T = 0.432$ for the following figures. (The calculation domain is larger than the represented area.)

the disturbance total kinetic energy and the disturbance total enstrophy respectively as:

$$E_c = \frac{1}{2} \iint_{\mathcal{D}} (\nabla\psi)^2 dx dy - E_{cu},$$

$$E_s = \frac{1}{2} \iint_{\mathcal{D}} (\nabla\psi)^2 dx dy,$$

where \mathcal{D} is the domain area and E_{cu} is the undisturbed flow non-dimensional kinetic energy.

In figure 7 we present E_c as a function of time for the three main typical regimes:

- For smallest values of μ , case (a), the energy E_c increases smoothly at first, crosses a maximum and afterwards becomes quite constant. This is observed even for values above the critical value μ_c corresponding to the Taylor-column appearance. The energy maximum is not associated with any particular physical event, but is only the combination of two opposite effects; trapping and shedding. On the contrary, the enstrophy maximum corresponds to the ultimate position of the two paired eddies on the topography; their separation causes a fast enstrophy decay.
- When μ is in the narrow range of values immediately larger than the previous ones, about $11 < \mu < 13$ for $r = 0$, the energy curve presents an inflexion before reaching its maximum, case (c). This inflexion arises at the same time that the enstrophy itself reaches its maximum value, that is to say when the eddies are paired (figures 4 and 8). The duration of this stage can be

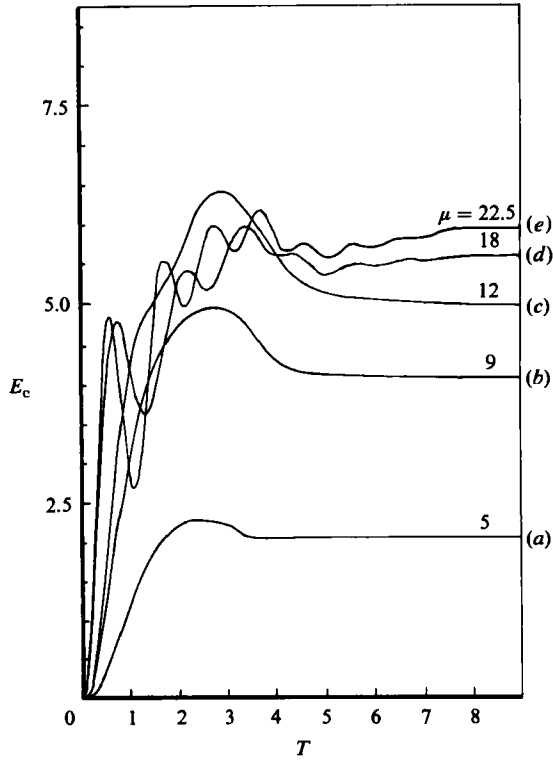


FIGURE 7. Perturbation energy E_c as a function of time T : $\beta = 0$; $r = 0$; $A = 0.005$.

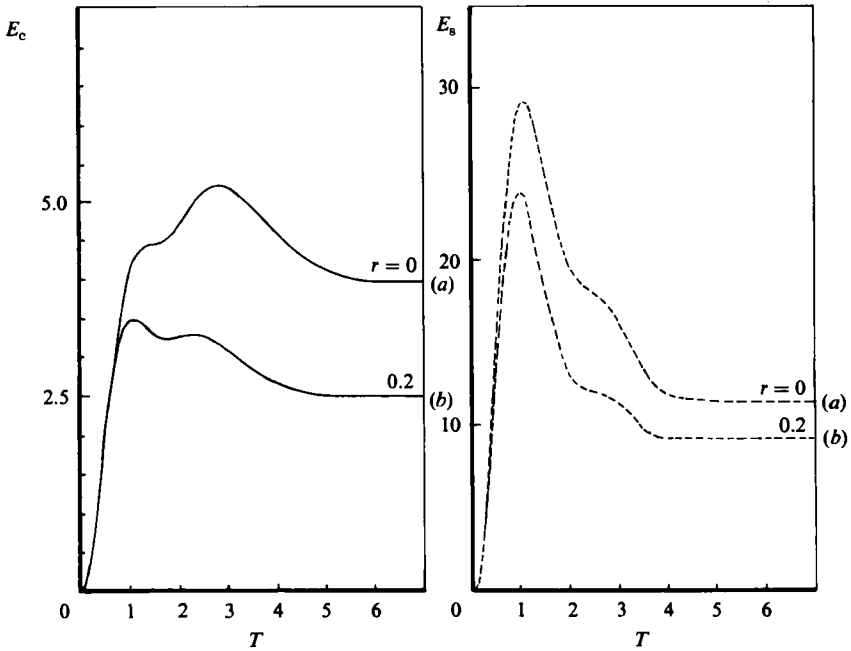


FIGURE 8. Perturbation energy E_c and enstrophy E_s versus time T bottom friction influence, $\mu = 12.5$; $\beta = 0$; $A = 0.01$.

understood as the lifetime of the paired eddies. The E_c and E_s subsequent variations are similar to the previous case.

- For largest values of μ , large-amplitude oscillations appear more intensively for energy than for enstrophy. As before, the energy passes through a maximum, but this happens after several oscillations whose period is that of the trapped circular waves' normal modes which have been already pointed out and will be examined at the end of this section.

The graphs in figures 7 and 8 case (a) are drawn for the case where bottom friction is negligible ($r = 0$). Nevertheless the main behaviour is the same if this assumption is not made, except that we obtain smaller levels for energy and enstrophy (figure 8b). Ekman pumping in the bottom boundary layer is reducing the vorticity generated on the topography, but a trapping effect still exists. The shed-eddy downstream motion is slackened; but the vorticity interaction is also reduced because the vorticity structures are less intense for a given advection. Moreover, the bottom friction allows stagnant fluid inside the closed streamlines to be really obtained: one can speak about the Taylor column with its original meaning when the flow is established.

The turbulent-viscosity influence is more difficult to identify partially because of the ambiguity of the turbulent-viscosity concept, and its role in modelling the dissipation of enstrophy at high wavenumbers. However the diffusive mechanism explains the destabilization of the solution with two paired eddies, which leads to the unique eddy solution after a long time. The solutions studied by Johnson (1977, 1978) and Kozlov (1981), in particular, could not last for a real fluid.

The two dissipative mechanisms, bottom and lateral friction, have timescales much larger than that characteristic of the flow. The viscous timescale is typically of the order of several years compared to an advective timescale which can extend from a few to ten days. Although the bottom friction will probably be the primary mechanism for energy dissipation (Holland 1978), and in spite of existing works on the bottom boundary layer, no satisfying parametrization is available; nevertheless the bottom-friction characteristic timescale is probably large compared to the advective timescale. Consequently in the context of oceanic flows, we can ensure that these dissipation processes do not modify the main aspects and chronology of the regimes, presented before for any given value of μ .

The diagrams in figures 9 and 10 present the energy and enstrophy variations versus the parameter μ , assuming the viscous dissipation is similar and the bottom friction is zero. The retained value for the kinetic energy E_c is the value which is obtained in a quasi-steady regime. In the enstrophy diagram we represent in addition the maximum value reached for each trial. This value corresponds to the critical position of the two paired-eddies solution. We can see on these E_c and E_s curves a change in the evolution of their slopes as soon as we go over the level $\mu = \mu_c$ where μ_c corresponds to the steady-state criterion for the Taylor-column initiation. That means that a part of the flow which was present initially on the topography, cannot pass over it and then is diverted around. Beyond this level a part of the flow is somewhat inhibited. For a large range of μ ($\mu > \mu_c$), this inhibition stays weak but for bigger values the inhibition role is really taking a dynamical predominance. We can thus see that:

- if $\mu \leq \mu_c$, E_c and E_s are growing according to a law close to the theoretical law issued from the analytical calculation $E_c \sim \mu^2$ and $E_s \sim \mu^2$;
- if $\mu > \mu_c$, we reach a roughly standing level for both energy and enstrophy. These quantities increase very slowly and become quite constant for the largest values of μ . This behaviour can be explained by the fact that the mean

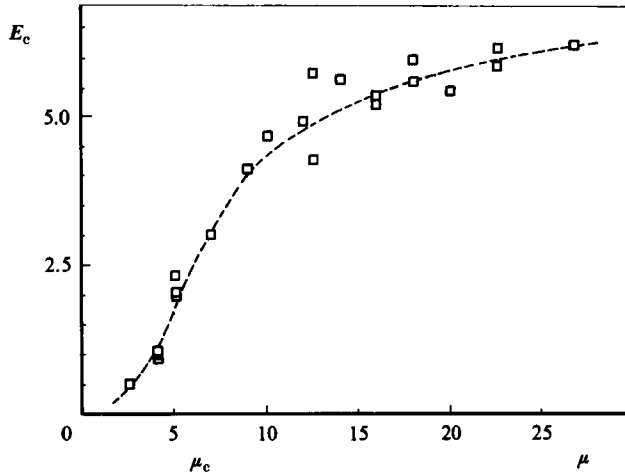


FIGURE 9. Perturbation energy E_c versus μ : $\beta = 0$; $r = 0$.

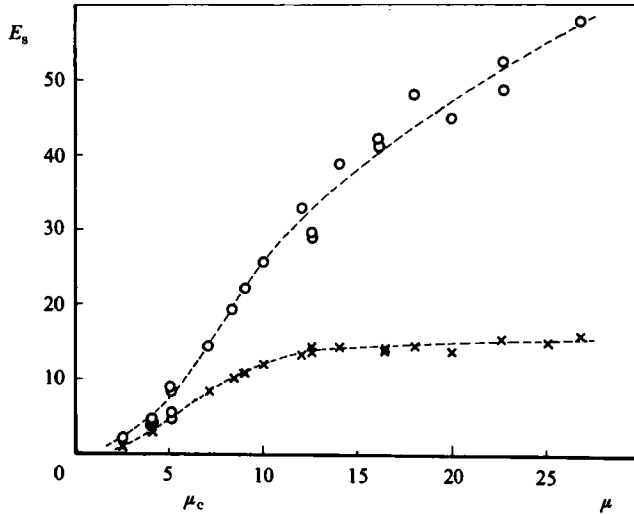


FIGURE 10. Perturbation enstrophy E_s versus μ : quasi-steady (\times); maximum value (\circ); $\beta = 0$; $r = 0$.

flow velocity which passes over the topography will become a smaller and smaller part of the global mean flow velocity for increasing μ . The mean velocity which is really 'felt' by the seamount (and which is generating the disturbance energy and enstrophy) is almost constant and keeps a value close to the one it has when $\mu = \mu_c$.

We have noted from figure 7 the existence of strong oscillations of the flow for big values of μ . The structure of these transient features is particularly clear on the vorticity field, as illustrated by figure 6: a part of the positive vortex shed on the right of the topography during the period of flow initiation (figure 6*a*) enters the anticyclonic vortex centred over the bump and seems to be trapped and to travel around it (figures 6*b, c, d*). A more detailed analysis of vorticity and stream-function patterns suggests some wavelike perturbation with two azimuthal modes and a phase

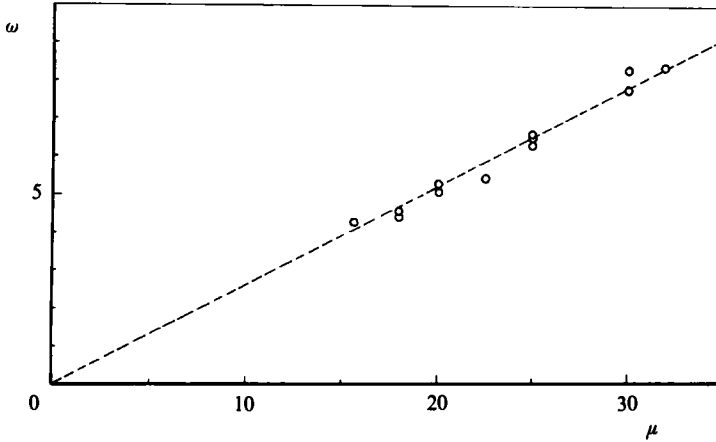


FIGURE 11. Circular wave frequency versus μ , first mode frequency: $\beta = 0$; $\tau = 0$.

moving clockwise around the topography. Rhines (1969) has computed such a quasi-geostrophic wave solution around paraboloidal seamounts looking radially like Bessel functions, and with one or several azimuthal modes; for these solutions, the dispersion relation implies an almost linear increase of the wave frequency with the relative height of the topography. From the curves of energy perturbation, typically as shown on figure 7, it is possible to identify the periodicity of these trapped waves, and we have plotted on figure 11 the corresponding frequency ω , related to the μ parameter. We can see the effective linear relation between ω and μ for the set of experiments which has been done in the present context.

5. β -Plane flow

In many problems of geophysical relevance the horizontal lengthscales are not small enough to justify the hypothesis that the latitudinal variation of the Coriolis parameter does not affect the dynamics.

When the β -effect is taken into account, the flow configuration looks markedly different because a Rossby wave pattern can be excited. Owing to the β -effect, a large area will now be affected by the disturbance, and not only a region close to the bump. In contrast to the f -plane case, the flow direction becomes a parameter and we are led to consider both eastward and westward flow.

5.1. Eastward flow

A wave pattern is excited mainly downstream of the obstacle but with a small component moving upstream. This system is superimposed on the f -plane configurations which we presented previously, although the critical values which determine regime transition are a little higher.

The dispersion relation derived from the steady linear equation (Lighthill 1967) for inviscid fluid can be written:

$$\sigma = -K_1 = -\frac{\beta K_1}{K_1^2 + K_2^2},$$

and gives us two solutions.

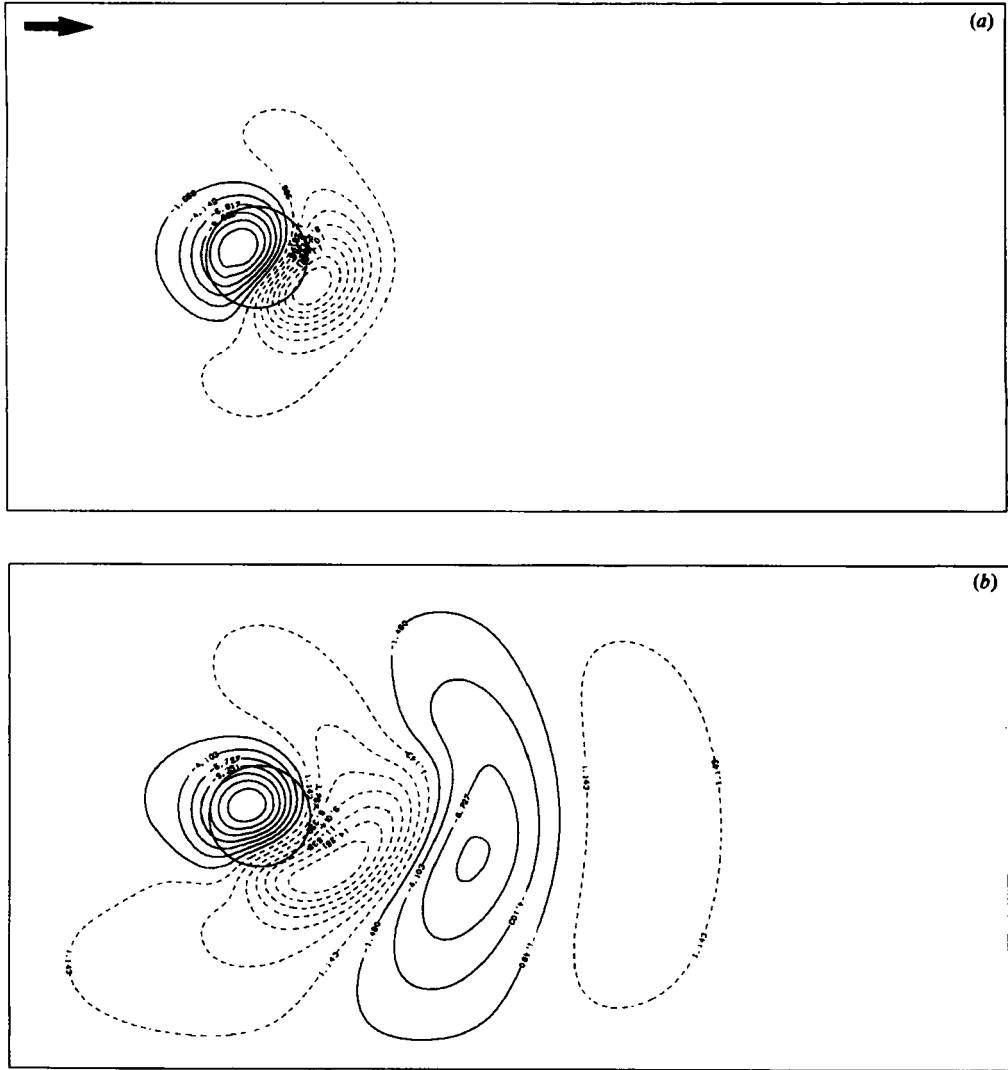


FIGURE 12(a,b). For caption see facing page.

The first one is defined by the wavenumber K such that:

$$|K|^2 = K_1^2 + K_2^2 = \beta,$$

and thus the non-dimensional wavelength is:

$$\lambda = \frac{2\pi}{\sqrt{\beta}}.$$

It corresponds to a circular-crest steady wave, whose group velocity is the incoming flow velocity. The lateral spreading of the wave pattern is fast and rapidly influenced by the solid boundaries of our domain. Thus we must expect that consecutive reflections of Rossby waves will give a complex network of incident and reflected waves.

The second solution is the zonal one with a zero frequency, but, depending on the

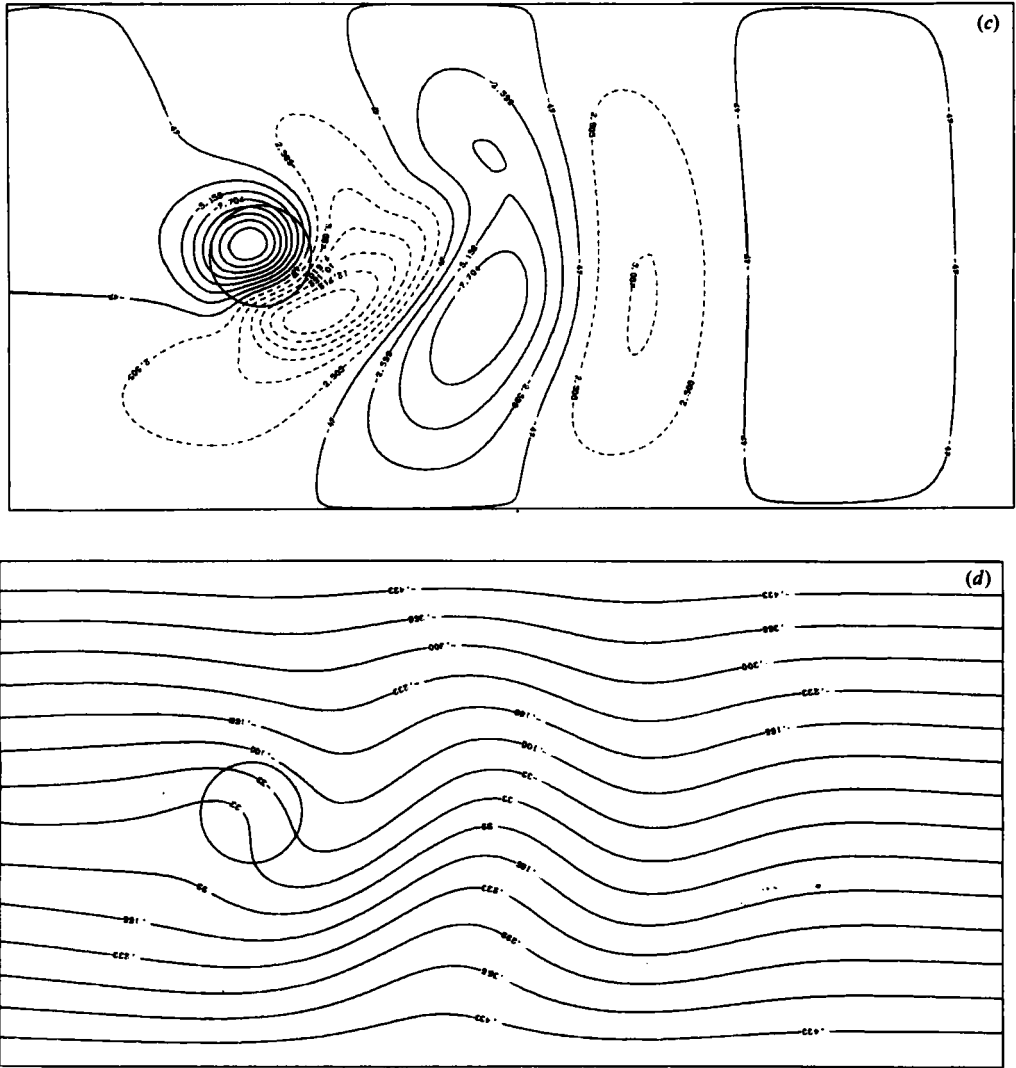


FIGURE 12. Vorticity field and streamlines, Rossby wave pattern for eastward flow: $\mu = 5$; $\beta = 4$; $r = 0.02$; $A = 0.01$. (a) At time $T = 0.72$; (b), 2.16; (c, d), 2.88.

wavelength in the meridional direction, the group velocity will become negative or positive. Indeed this velocity is defined as:

$$C_g = 1 - \frac{\beta}{K_2^2},$$

so all the zonal structures where the non-dimensional wavelength is more than $\lambda_0 = 2\pi/\sqrt{\beta}$ will propagate upstream. The smallest structures with wavelength less than λ_0 will propagate downstream like the main trailing wave pattern. The biggest zonal waves represent a steady current which can go against the main flow and then decrease it. In that case, the existence of the upstream open boundary is clearly advantageous.

In figure 12 we can observe an example of β -plane flow which behaves like those

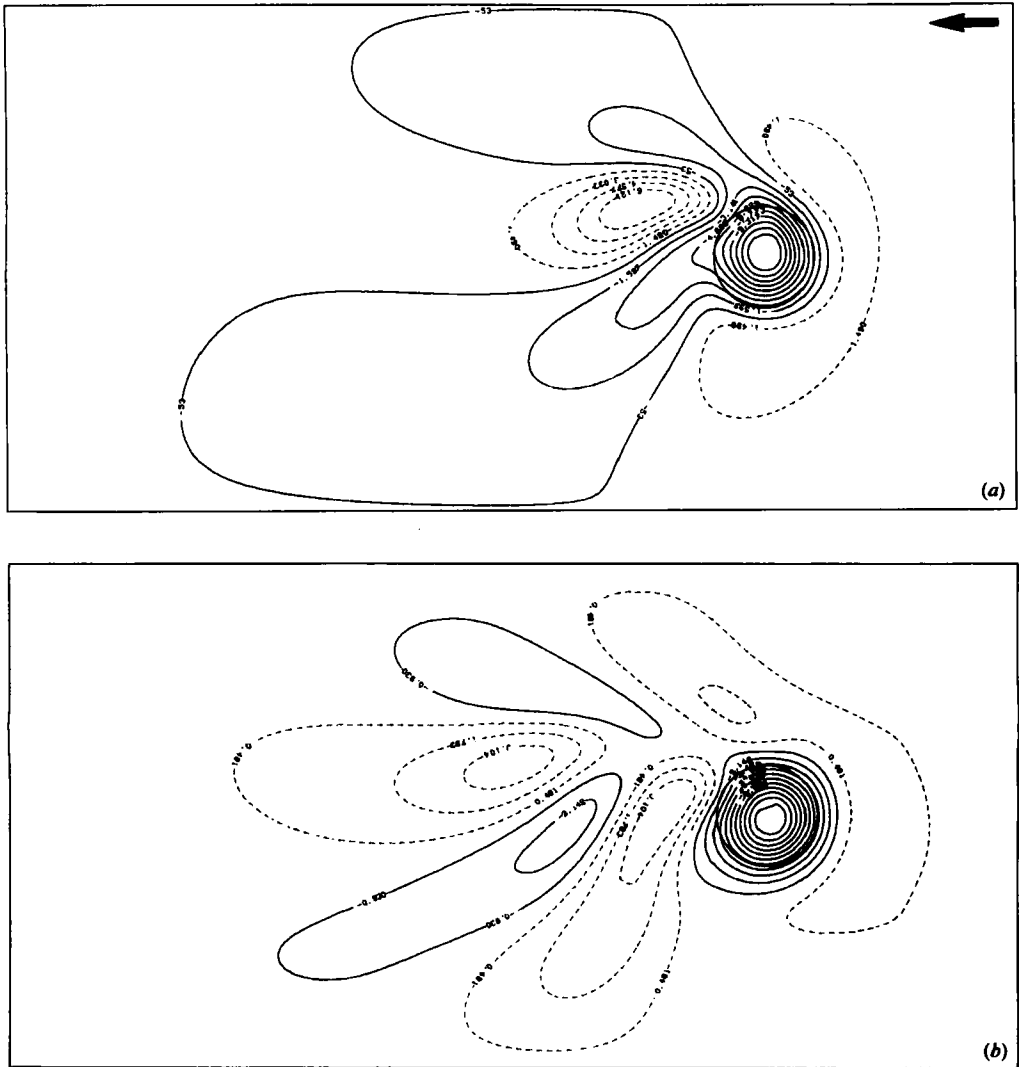


FIGURE 13(a, b). For caption see facing page.

previously described. Downstream the stationary Rossby wave is progressively extending with a group velocity approximately equal to U . Upstream the first transverse mode can be guessed although the zonal waves' initiation is occurring rapidly during the first time-steps. Nevertheless the small induced countercurrent is clearly observed in front of the bump through the streamlines' spacing. (When the open boundary is missing, a strong distortion of the upstream streamlines appears because of the blocking of these structures.)

In the vicinity of the bump, it is clear that the β -effect does not affect the vortex-stretching primary mechanism and the occurrence of two vorticity structures on the topography. However the eddies' rotation in the clockwise sense seems to be favoured. This local effect coupled to the energy radiation by Rossby waves can explain the small displacement of the μ range for regime transition.

For the largest values of μ , the trapping of the two vorticity areas is accompanied by oscillations, as already mentioned with respect to the f -plane (figure 6). In that

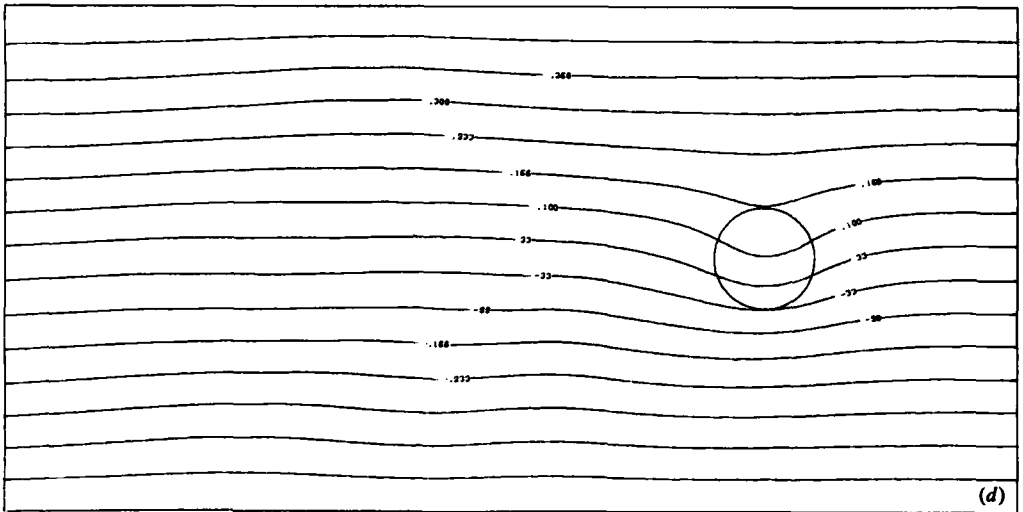
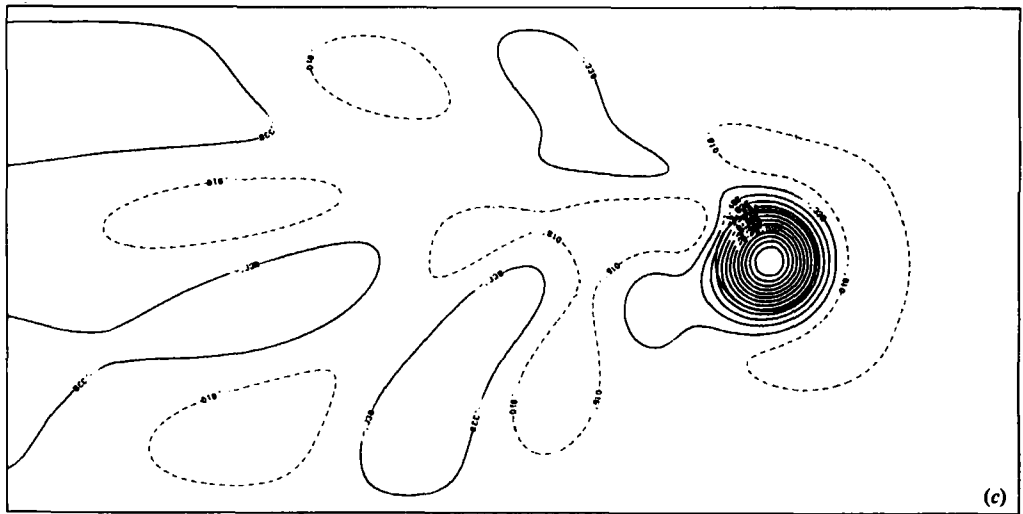


FIGURE 13. Vorticity field and streamlines, zonal wave pattern for westward flow: $\mu = 5$; $\beta = 4$; $r = 0$; $A = 0.01$. (a) At time $T = 1.44$; (b), 2.30; (c, d), 4.32.

case, the zonal wave excitation can last longer, and the induced countercurrent appears to be more intense.

The first mode of the trapped oscillations, computed from the energy-variation curves, has a frequency which is very near to the corresponding f -plane frequency. It agrees with Rhines' (1969) hypothesis that the β -effect can be neglected locally over such a mesoscale topography.

5.2. Westward flow

Forcing in the retrograde direction does not allow the excitation of Rossby waves and the flow configuration is very near to the f -plane configuration. The β -effect reinforces the trapping of the negative-vorticity core on the topography. The steadiness of such a situation is rapidly obtained after exciting transient disturbances. These small-amplitude disturbances propagate upstream and principally downstream.

As in the eastward case, they can be interpreted as topography-excited waves. In that sense, the disturbance corresponds to the trivial solution (and only in that case) of the dispersion relation. The group velocity of these waves exceeds that of the incoming flow whatever the wavenumber. Consequently all the zonal waves will travel westward and not only the big structures, as before. The last ones have much larger group velocities and will leave the domain quickly. We present an example in figure 13 where we can clearly observe the initiation of the first odd mode in the transverse direction (figure 13*a*), followed by the second odd mode (figure 13*b*).

6. Summary

The detailed analysis of the extensive set of numerical experiments performed with the open-boundary model described in this paper has led to an overview of the different classes of transient regimes which can occur when homogeneous viscous flow is impinging on an isolated topography in a rotating system.

In the f -plane case, it is shown that the ultimate solution is always characterized by a typical vorticity field with an anticyclonic vortex trapped over the topography; the intensity of this vortex is related to the importance of the topography, but limited by the Taylor-column formation process. Different transient regimes occur, however: for strong flows, the positive vortex generated in the initiation flow phase is directly advected downstream; for weak flows a stronger interaction between the two eddies occurs and the positive vortex is shifted to the right and trapped in the vicinity of the bump, leading to a double-vortex structure. All these features fit with the description given by Huppert & Bryan (1976) and Johnson (1978), among others. When the vorticity interaction is very strong, the positive vorticity field enters the anticyclonic eddy and excites wavelike smaller-scale vorticity structures trapped and travelling around the bump, just like topographic trapped waves identified by Rhines (1969). In all these cases, after a time, and because of vorticity diffusion, the vorticity interactions weaken and the positive field ends by escaping the vicinity of the hill and drifting with the oncoming flow.

In the β -plane case and for prograde flows, similar regimes occur, but are complicated by the presence of Rossby waves, extending downstream under a stationary wave pattern, and upstream as zonal currents. For retrograde flows, only transient zonal waves are observed downstream.

The authors wish to thank A. Colin de Verdière, H. E. Huppert, D. B. Haidvogel and the referees for their valuable comments. Part of the calculations have been made with the numerical facilities of the Centre de Calcul Vectoriel pour la Recherche in Palaiseau.

REFERENCES

- ARAKAWA, A. 1966 Computational design for long term integration of the equations of fluid motions. *J. Comp. Phys.* **1**, 119–143.
- BAINES, P. G. & DAVIES, P. A. 1980 Laboratory studies of topographic effects in rotating and/or stratified fluids. *Orographic Effects in Planetary Flows*, pp. 233–299. GARP Publications series no. 23.
- BOYER, D. L. & DAVIES, P. A. 1982 Flow past a circular cylinder on a β -plane. *Phil. Trans. R. Soc. Lond. A* **306**, 533–556.
- BOYER, D. L., DAVIES, P. A. & HOLLAND, W. R. 1984 Rotating flow past disks and cylindrical depressions. *J. Fluid Mech.* **141**, 67–95.

- DAVIES, P. A. 1972 Experiments on Taylor columns in rotating stratified fluids. *J. Fluid Mech.* **54**, 691–717.
- GOULD, W. J., HENDRY, R. & HUPPERT, H. E. 1981 An abyssal topographic experiment. *Deep-Sea Res.* **28 A**, 409–440.
- HIDE, R. 1961 Origin of Jupiter's Great Red Spot. *Nature* **190**, 895–896.
- HIDE, R. & IBBETSON, A. 1966 An experimental study of Taylor columns. *Icarus* **5**, 279–290.
- HIDE, R., IBBETSON, A. & LIGHTHILL, J. 1968 On slow transverse flow past obstacles in a rapidly rotating fluid. *J. Fluid Mech.* **32**, 251–272.
- HOCKNEY, R. W. 1971 The potential calculation and some applications. *Methods in Comp. Phys.* **9**, 135–211.
- HOGG, N. G. 1973 On the stratified Taylor column. *J. Fluid Mech.* **58**, 517–537.
- HOLLAND, W. R. 1978 The role of mesoscale eddies in the general circulation of the ocean. Numerical experiments using a wind-driven quasi-geostrophic model. *J. Phys. Oceanogr.* **8**, 363–392.
- HUPPERT, H. E. 1975 Some remarks on the initiation of inertial Taylor columns. *J. Fluid Mech.* **67**, 397–412.
- HUPPERT, H. E. & BRYAN, K. 1976 Topographically generated eddies. *Deep-Sea Res.* **23**, 655–679.
- INGERSOLL, A. P. 1969 Inertial Taylor columns and Jupiter's Great Red Spot. *J. Atmos. Sci.* **26**, 744–752.
- JAMES, I. N. 1980 The forces due to geostrophic flows over shallow topography. *Geophys. Astrophys. Fluid Dyn.* **14**, 225–250.
- JOHNSON, E. R. 1977 Stratified Taylor columns on a beta-plane. *Geophys. Astrophys. Fluid Dyn.* **9**, 159–177.
- JOHNSON, E. R. 1978*a* Trapped vortices in rotating flow. *J. Fluid Mech.* **86**, 209–224.
- JOHNSON, E. R. 1978*b* Quasigeostrophic flow above sloping boundaries. *Deep-Sea Res.* **25**, 1049–1071.
- JOHNSON, E. R. 1978*c* Topographically bound vortices. *Geophys. Astrophys. Fluid Dyn.* **11**, 61–71.
- JOHNSON, E. R. 1979 Finite depth stratified flow over topography on a beta-plane. *Geophys. Astrophys. Fluid Dyn.* **12**, 35–43.
- KOZLOV, V. F. 1981 On a stationary problem of topographical cyclogenesis in a homogeneous rotating fluid. *Izv. Atmos. and Ocean. Phys.*, vol. 17, no. 11.
- KREISS, H. O. 1966 In *Proc Symp. University of Wisconsin*, (ed. Donald Greenspan). Wiley.
- LIGHTHILL, M. J. 1967 On waves generated in dispersive systems by travelling forcing effects, with applications to the dynamics of rotating fluids. *J. Fluid Mech.* **27**, 725–752.
- MCCARTNEY, M. S. 1975 Inertial Taylor columns on a beta-plane. *J. Fluid Mech.* **68**, 71–95.
- MEINCKE, J. 1971 Observation of an anticyclonic vortex trapped above a seamount. *J. Geophys. Res.* **76**, 7432–7440.
- ORLANSKI, I. 1976 A simple boundary condition for unbounded hyperbolic flows. *J. Comp. Phys.* **21**, 251–269.
- OWENS, W. B. & HOGG, N. G. 1980 Oceanic observations of stratified Taylor columns near a bump. *Deep-Sea Res.* **27 A**, 1029–1045.
- PEDLOSKI, J. 1979 *Geophysical Fluid Dynamics*. Springer-Verlag.
- PROUDMAN, J. 1916 On the motion of solids in a liquid possessing vorticity. *Proc. Roy. Soc. Lond.* **A 92**, 408–424.
- RHINES, P. B. 1969*a* Slow oscillations in an ocean of varying depth. Part 1: Abrupt topography. *J. Fluid Mech.* **37**, 161–189.
- RHINES, P. B. 1969*b* Slow oscillations in an ocean of varying depth. Part. 2: Islands and seamounts. *J. Fluid Mech.* **37**, 191–205.
- RICHARDSON, P. L. 1980 Anticyclonic eddies generated near the Corner Rise seamounts. *J. Mar. Res.* **38**, 673–686.
- SCHMITZ, W. J. & HOLLAND, W. R. 1982 A preliminary comparison of selected numerical eddy resolving general circulation experiments with observations. *J. Mar. Res.* **40**, 75–117.
- TAYLOR, G. I. 1917 Motion of solids in fluids when the flow is not irrotational. *Proc. Roy. Soc. Lond.* **A 93**, 99–113.

- VASTANO, A. C. & WARREN, B. A. 1976 Perturbations to the Gulf Stream by Atlantis II. Seamount. *Deep-Sea Res.* **23**, 681–694.
- VAZIRI, A. 1977 Topographic effects of rotating flows on a beta-plane. *Recent Advances in Engng Sci.* **8**, 205–214.
- VAZIRI, A. & BOYER, D. L. 1971 Rotating flow over shallow topographies. *J. Fluid Mech.* **50**, 79–95.